We are IntechOpen, the world's leading publisher of Open Access books Built by scientists, for scientists

4,800
Open access books available

122,000
International authors and editors

135M
Downloads

Our authors are among the

154
Countries delivered to

TOP 1%
most cited scientists

12.2%
Contributors from top 500 universities

CLARIVATE ANALYTICS BOOK CITATION INDEX INDEXED

WEB OF SCIENCE™

Selection of our books indexed in the Book Citation Index in Web of Science™ Core Collection (BKCI)

Interested in publishing with us?
Contact book.department@intechopen.com

Numbers displayed above are based on latest data collected.
For more information visit www.intechopen.com

2

Advances in Multistatic Sonar

Danilo Orlando[1] and Frank Ehlers[2]
[1]*Dipartimento di Ingegneria dell'Innovazione - Università del Salento*
[2]*NATO Undersea Research Centre*
Italy

1. Introduction

Although the concept of multistatic active sonar (MAS) has been around for over 50 years, new trends have brought this technology to the forefront of anti-submarine warfare research. These trends include advancements in sonar sensors and signal processing, advancements in submarine stealth, and a desire to track targets in noisy and reverberant environments, such as near-shore or shallow waters. The latest trend is to exploit the really game-changing capabilities of unmanned and autonomously operating underwater vehicles.

The focus of this chapter is on advances in signal processing enabling especially the tracking of low signature targets, namely targets with low signal-to-noise ratio (SNR), in a multisensor environment. In particular, the track-before-detect (TBD) approach and its adaption to pre-selected contact-based tracking are addressed. The TBD approach is designed to track low SNR targets. TBD-based procedures jointly process several consecutive pings and, relying on target kinematics or, simply, exploiting the physically admissible target transitions, declare the presence of a target and, eventually, its track (Orlando et al., IEEE-TSP 2010). A TBD algorithm is typically fed by unthresholded data or thresholded data with significantly lower thresholds than the ones used by conventional trackers. Moreover an important feature of a TBD scheme is the so-called constant false track acceptance rate (CFTAR) property: if a TBD scheme ensures the constant false alarm rate property with respect to the unknown statistics of the disturbance, then it allows controlling the overall false track acceptance rate. The TBD algorithm herein presented considers a bistatic sonar architecture and is capable of handling raw hydrophone data (Orlando et al., CIP 2010). Remarkably, it guarantees the CFTAR property. Performance analysis highlights its potential to implement automatic track continuation and to prepare automatic classification for temporarily weak targets as these tasks are usually the challenges that MAS systems have to overcome.

In the context of multistatic sonar, a batch algorithm is also introduced, that jointly processes measurements provided by multiple sensors over a certain number of consecutive pings (Orlando et al., FUSION 2010). These measurements are time differences of arrival and bearing information of a target maneuvering in the surveillance region. This approach is tested on a benchmark data set provided by METRON in the context of collaborative international multi-laboratory research that is ongoing in the ISIF Multi-Static Tracking Working Group (Orlov, Metron Data set 2009).

The remainder of this chapter is organized as follows: the next section is devoted to the description of bistatic and multistatic sonar systems. Section III focuses on the derivation of the TBD (or TBD-based) processors. In Section IV a node selection strategy for multistatic

sonar systems is described on a conceptual level while Section V provides some illustrative examples. Finally, Section VI contains concluding remarks and hints for future work.

2. Multistatic sonar

When low frequency active sonar was first used to find and track underwater targets, the required hardware for both the acoustic source and the acoustic receiver was installed onboard a single unit. The deployed part (or wet-end) of the system is quite heavy and large in extend and there has to be a synchronization between the activating source and the receiving hydrophones. Hence, the natural approach is to use such a monostatic system (source and receiver collocated) in order to avoid the necessity and cost for multiple units involved and data synchronization issues. However, looking at the cylindrical structure of the target it turns out that approaching or opening aspects of the target result in very low detection probabilities for those monostatic systems.
An enormous improvement in performance is possible if multiple acoustic sources and receivers are deployed in a spatially distributed manner. Multiple units have to be used and data synchronization has to be solved in order to implement these so called multistatic active sonar systems. A multistatic architecture can provide:

- short latency (due to effective Doppler processing);
- high precision (due to triangulation);
- fewer false alarms;
- anti-stealth.

These benefits can only be exploited by automatic fusion and tracking of the multistatic data. Automatic tracking algorithms use the information from consecutive measurements to discriminate between physically feasible movements and random movements of prospective targets. By this discrimination the overall false alarm rate can be reduced, especially when different bistatic aspects on the target are combined within the tracking algorithm. It is possible to summarize the major issues of MAS as follows:

1. estimation task: non-linear and noisy measurements and variable sound channels;
2. multi-target issue: false alarms, clutter targets, and bottom reflections;
3. non-cooperative evader: stealthy target with evading actions;
4. multi-agent coordination whereby communication between sensors needed, but not always present.

In this chapter, two TBD-based techniques are introduced in order to overcome limitations due to the issues 1 and 2.
Before proceeding further, notice that a multistatic system consists of multiple sources and multiple receivers and, hence, it can be viewed as composed of different bistatic subsystems. For this reason, the bistatic configuration is first introduced in Subsection 2.1, then the description of the multistatic architecture is given in Subsection 2.2.

2.1 System description: the bistatic architecture

The bistatic sonar scenario involves a projector and a receiver, placed at a different location and equipped with an array of sensors, a point-like target at a certain "distance" from the array (range), and a signal that travels from the projector to the target and from the target to the receiver. The system under consideration utilizes a planar array (see Figure 1) consisting of

N_a arms; each of them contains N_s identical sensors spaced d meters apart from one another. The total number of sensors is

$$N = N_a(N_s - 1) + 1, \tag{1}$$

where we are accounting for the fact that the arms share the central sensor. Moreover, let $\theta_a = 2\pi/N_a$ be the separation angle between two consecutive arms, θ_r the azimuthal angle of the impinging target echo, measured clockwise from the reference arm, and

$$\theta_i = \theta_r - (i-1)\theta_a, \quad i = 1, \ldots, N_a, \tag{2}$$

the angle of arrival with respect to the ith arm.
Suppose that the projector omnidirectionally transmits the following pulse waveform

$$\Re e\left\{ A e^{j\phi} p(t) e^{j2\pi f_c t} \right\}, \quad t \in [0,\ T_p[, \tag{3}$$

where

$$p(t) = \frac{1}{\sqrt{T_p}} e^{j\pi k t^2} \tag{4}$$

is a frequency modulated waveform of duration T_p, $A > 0$ is an amplitude factor related to the transmitted power, $\phi \in [0, 2\pi[$ is the initial phase of the carrier signal, f_c is the carrier frequency, $\Re e\{z\}$ denotes the real part of the complex number z, and $k = B/T_p$, with B the pulse bandwidth. In the next subsection, we derive the discrete-time form for the received signal.

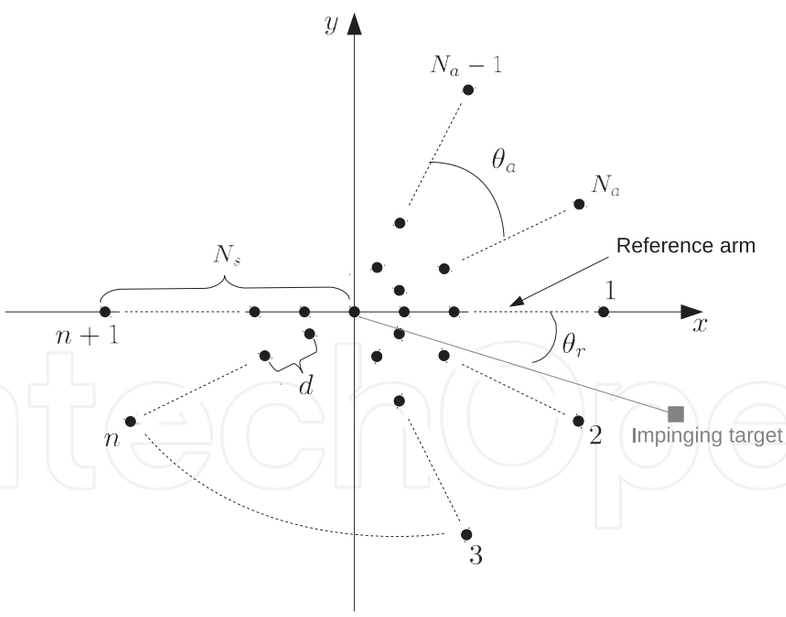

Fig. 1. The planar array and the associated reference system: each sensor is represented by a filled circle.

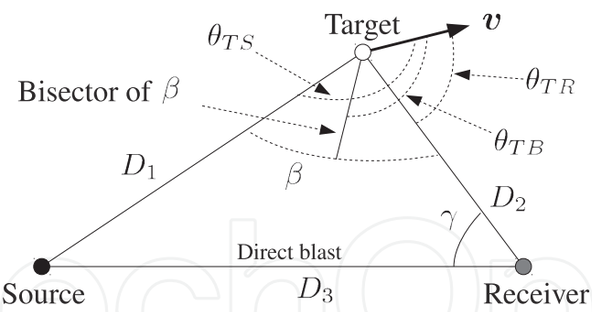

Fig. 2. Bistatic geometry

2.1.1 Discrete-time sensor model

Consider the geometry depicted in Figure 2 and suppose that a prospective (point-like) target is moving within the surveillance area with a velocity vector $\boldsymbol{v} \in \mathbb{R}^{2\times 1}$. The received signal at the nth sensor of the ith arm is given by

$$r_{n,i}(t) = \mathfrak{Re}\left\{ \frac{\alpha}{\sqrt{T_p}} e^{j\pi k(t-\tau_{n,i}(t))^2} e^{j2\pi f_c(t-\tau_{n,i}(t))} \right\} + n_{n,i}(t), \tag{5}$$

where

- $\alpha \in \mathbb{C}$ is a complex and unknown (deterministic) factor accounting for the transmitted power, the transmitting and receiving gain, the two-way path loss, and the sonar cross-section of the target; hereafter α denotes any proper modification of the previous constant;
- $\tau_{n,i}(t)$ is the time delay between the transmission by the source and the arrival of the target echo at the nth sensor of the ith arm;
- $n_{n,i}(t)$ is the overall disturbance component; in the sequel we use the above symbol to denote any modification of the noise components.

Now observe that $\tau_{n,i}(t)$ consists of three components

$$\tau_{n,i}(t) = \tau_1(t) + \tau_2(t) - \frac{d(n-1)}{c}\cos\theta_i, \tag{6}$$

where[1] c ($\gg \|\boldsymbol{v}\|$) is[2] the speed of sound in water, $\tau_1(t)$ is the travel time of the transmitted signal from source to target, and $\tau_2(t)$ is the travel time of the target echo from target to receiver[3].

For the sake of convenience, it is worth defining the following time difference of arrival

$$\tau'(t) = \tau_1(t) + \tau_2(t) - \tau_3, \tag{7}$$

where $\tau_3 = D_3/c$ is the travel time from source to receiver (D_3 is the distance between the source and the receiver). It follows that equation (5) can be recast as

$$r_{n,i}(t) \approx \mathfrak{Re}\left\{ \alpha e^{j\pi k(t-\tau'(t)-\tau_3)^2} e^{j2\pi f_c t} e^{j2\pi(n-1)\nu_i} e^{-j2\pi f_c \tau_3} e^{-j2\pi f_c \tau'(t)} \right\} + n_{n,i}(t), \tag{8}$$

[1] Recall that d is the interelement spacing

[2] $\|\cdot\|$ denotes the Euclidean norm.

[3] To be more precise, $\tau_2(t)$ is the travel time of the target echo from the target to the origin of the reference system which coincides with the center of the receiver (see Figure 1).

where

$$\nu_i = \frac{d}{\lambda}\cos\theta_i \tag{9}$$

is the *spatial frequency* with respect to the ith arm. An equivalent monostatic range $D'(t)$, corresponding to $\tau'(t)$, can be defined as follows

$$D'(t) = \frac{c\tau'(t)}{2} = D' - v'\left(t - \frac{\tau'(t)}{2}\right), \tag{10}$$

where D' is the initial equivalent monostatic range and (Willis, Scitech Pub. 2005)

$$v' = \|v\|\cos\theta_{TB}\cos\frac{\beta}{2}(< \|v\| \ll c). \tag{11}$$

Equation (11) can be obtained by writing $D'(t)$ as follows

$$D'(t) = \left[\frac{D_1(t) + D_2(t) - D_3}{2}\right], \tag{12}$$

where $D_1(t)$ is the source-target distance and $D_2(t)$ is the receiver-target distance, and evaluating its first derivative with respect to t, namely

$$\frac{d}{dt}D'(t) = \frac{1}{2}\|v\|(\cos\theta_{TR} + \cos\theta_{TS}), \tag{13}$$

where

$$\theta_{TR} = \theta_{TB} - \beta/2, \tag{14}$$

$$\theta_{TS} = \theta_{TB} + \beta/2. \tag{15}$$

It is not difficult to show that knowledge of D' and θ_r allows to evaluate the initial receiver-target distance, D_2 say. Indeed, from Figure 2 the following relation among the initial source-target distance, D_1 say, D_2, and D_3 holds true

$$D_1^2 = D_2^2 + D_3^2 - 2D_2D_3\cos\gamma. \tag{16}$$

Then, solving the next equation

$$D' = \frac{D_1 + D_2 - D_3}{2} \tag{17}$$

with respect to D_1 and substituting the solution into (16) yields

$$D_2 = D'\left[\frac{1 + D_3/D'}{1 + (D_3/D')(1-\cos\gamma)/2}\right]. \tag{18}$$

The above equation allows us to recast the expression of the received signal in terms of the equivalent monostatic quantities v', D', and $\tau'(t)$. More specifically, from equation (10) we obtain

$$\tau'(t) \approx \frac{2D'}{c} - \frac{2v't}{c} = \tau' - \frac{2v't}{c}, \tag{19}$$

where[4]

$$\tau' = \frac{2D'}{c}. \tag{20}$$

[4] Remember that $c \gg v'$.

Then, inserting (19) into (8) yields

$$r_{n,i}(t) \approx \Re e\left\{\alpha e^{j\pi k(t-\tau'-\tau_3)^2} e^{j2\pi f_c t} e^{j2\pi(n-1)\nu_i} e^{j2\pi f'_D t}\right\} + n_{n,i}(t), \tag{21}$$

where

$$f'_D = 2\frac{f_c v'}{c}. \tag{22}$$

After complex baseband conversion, the output of a filter matched to $p(t)$ is given by (see (Bandiera at al., M&C 2009))

$$y_{n,i}(t) = \alpha \int_{-\infty}^{+\infty} e^{j\pi k(u-\tau'-\tau_3)^2} e^{j2\pi(n-1)\nu_i} e^{j2\pi f'_D u} e^{-j\pi k(t-u)^2} du + n_{n,i}(t). \tag{23}$$

Let $u_1 = u - \tau' - \tau_3$, then

$$\begin{aligned} y_{n,i}(t) &= \alpha e^{j2\pi(n-1)\nu_i} \int_{-\infty}^{+\infty} e^{j2\pi f'_D u_1} e^{j\pi k u_1^2} e^{-j\pi k[u_1-(t-\tau'-\tau_3)]^2} du_1 + n_{n,i}(t) \\ &= \alpha \chi_p(t-\tau'-\tau_3, f'_D) e^{j2\pi(n-1)\nu_i} + n_{n,i}(t), \end{aligned} \tag{24}$$

where again α and $n_{n,i}(t)$ denote a proper modification of the target response and of the noise component, respectively, and $\chi_p(\cdot,\cdot)$ is the (complex) ambiguity function of $p(t)$.
In order to generate the vector of the noisy returns corresponding to the lth range gate, $l = 1, \ldots, L$, the output of the matched filter $y_{n,i}(t)$ is sampled at

$$t_l = t_{\min} + (l-1)T_B, \tag{25}$$

where $t_{\min}$ denotes the beginning of the sampling process and $T_B = 1/B$. The time samples are grouped to form an N-dimensional vector (recall that $N = N_a(N_s - 1) + 1$), as follows

$$\begin{aligned} \boldsymbol{z}_l &= [y_{1,1}(t_l) \cdots y_{N_s,1}(t_l)\, y_{2,2}(t_l) \cdots y_{N_s,2}(t_l) \cdots y_{2,N_a}(t_l) \cdots y_{N_s,N_a}(t_l)]^T \\ &= \boldsymbol{s}_l + \boldsymbol{n}_l, \end{aligned} \tag{26}$$

where

- ^{T} denotes transpose;
- $\boldsymbol{s}_l \in \mathbb{C}^{N\times 1}$ is the useful signal vector[5];
- $\boldsymbol{n}_l \in \mathbb{C}^{N\times 1}$ is the noise vector.

It is important to stress here that the bistatic range resolution is conventionally taken to be

$$\delta = c\frac{T_B}{2}. \tag{27}$$

However, two targets lying on the isorange contours must be at least physically separated by a distance given by

$$\frac{cT_B}{2\cos(\beta/2)} \tag{28}$$

to generate a separation δ at the receiver (Willis, Scitech Pub. 2005).

[5] $\boldsymbol{s}_l$ incorporates the complex amplitude α

Now, assuming that

$$\tau' + \tau_3 \in [t_{\min}, t_{\min} + (L-1)T_B], \tag{29}$$

it follows that

$$\exists \bar{l} \in \{1, \ldots, L-1\} : \tau' + \tau_3 = t_{\min} + (\bar{l}-1)T_B + \epsilon', \tag{30}$$

$0 \leq \epsilon' \leq T_B$, and, hence, that

$$\boldsymbol{s}_l = \begin{cases} \alpha \chi_p(-\epsilon', f'_D)\boldsymbol{v}(\theta_r), & l = \bar{l}, \\ \alpha \chi_p(T_p - \epsilon', f'_D)\boldsymbol{v}(\theta_r), & l = \bar{l}+1, \\ \mathbf{0}, & l \neq \bar{l}, \bar{l}+1, \end{cases} \tag{31}$$

where $\mathbf{0}$ is a null vector of proper dimensions and

$$\boldsymbol{v}(\theta_r) = \left[1 \; e^{j2\pi\nu_1} \; \ldots \; e^{j2\pi(N_s-1)\nu_1} \; \ldots \; e^{j2\pi\nu_{N_a}} \; \ldots \; e^{j2\pi(N_s-1)\nu_{N_a}}\right]^T \tag{32}$$

is the *spatial steering vector*.
In the following we assume that the target is located at the center of the lth range gate, namely that there is no spillover of target energy to adjacent matched filter samples. Thus, equation (31) becomes

$$\boldsymbol{s}_l = \begin{cases} \alpha \boldsymbol{v}(\theta_r), & l = \bar{l}, \\ \mathbf{0}, & l \neq \bar{l}. \end{cases} \tag{33}$$

A remark is now in order. Observe that the $\boldsymbol{z}_l$'s (equation (26)) are usually processed to generate the contacts used by conventional trackers. An alternative to the traditional approach consists in feeding the $\boldsymbol{z}_l$'s to a TBD processor that operates with raw data (see Subsection 3.1).

2.2 Contact-based multistatic architecture

This subsection is devoted to the description of a multisensor surveillance sonar system that processes thresholded data to track prospective targets. In particular, we focus our attention on a sensor network which provides a set of time difference of arrival (TDOA) and bearing information on M consecutive pings. Notice that each network node makes hard decisions and transmits these results to the fusion center for track estimate. In other words, we consider a parallel fusion network employing centralized fusion architecture (Varshney, Springer 1997).
The considered system consists of multiple acoustic sound sources and multiple receivers, more precisely

- N_{sr} sources that alternately illuminate the surveillance region with a ping occurring every T_{pg} seconds; the N_{sr}-source ping schedule is

$$n_{sr} = [(m-1) \mod N_{sr}] + 1, \tag{34}$$

  where n_{sr} is the index of the transmitting source at the mth ping and $[a \mod b]$, $a, b \in \mathbb{N}$, is the remainder of the division a/b.

- N_r synchronous omnidirectional receivers.

Source and receiver positions are known. Each receiver provides a set of measurements (or contacts), denoted as follows

$$Z_{i,m} = \{\boldsymbol{z}_{i,1,m}, \ldots, \boldsymbol{z}_{i,N_{i,m},m}\}, \quad i = 1, \ldots, N_r, \quad m = 1, \ldots, M, \tag{35}$$

where M is the total number of consecutive illuminations and $N_{i,m}$ is the number of measurements collected by the ith receiver at the mth ping. As to the $z_{i,j,m}$'s, they are 2-dimensional vectors defined as

$$z_{i,j,m} = \begin{bmatrix} d_{i,j,m} \\ \phi_{i,j,m} \end{bmatrix} \in \mathbb{R}^{2\times 1}, \tag{36}$$

where $\phi_{i,j,m}$ is the bearing measured clockwise from the receiver north and $d_{i,j,m}$ denotes the TDOA between the direct blast and the contact.

2.2.1 Sensor model

In the sequel, we assume that when a measurement has originated from the target, the errors for TDOA and bearing are independent zero-mean Gaussian random variables, namely

$$\Delta d_{i,j,m} \sim \mathcal{N}_1(0, \sigma_d^2) \quad \text{and} \quad \Delta\phi_{i,j,m} \sim \mathcal{N}_1(0, \sigma_\phi^2), \quad \forall i, j, m, \tag{37}$$

where $\sigma_d > 0$ and $\sigma_\phi > 0$ are the respective standard deviations and are supposed known.
On the other hand, when the contacts are due to the noise, we assume that they are uniformly distributed in the measurement space, i.e.,

$$d_{i,j,m} \sim \mathcal{U}(d_{i,m}^{\min}, d_{i,m}^{\max}) \quad \text{and} \quad \phi_{i,j,m} \sim \mathcal{U}(\phi_{i,m}^{\min}, \phi_{i,m}^{\max}), \tag{38}$$

where

- $d_{i,m}^{\min}$ and $\phi_{i,m}^{\min}$ denote the minimum values for TDOA and bearing, respectively;
- $d_{i,m}^{\max}$ and $\phi_{i,m}^{\max}$ are the maximum values for TDOA and bearing, respectively.

These parameters are tied to the application in question and to the employed technology, more precisely they can be chosen on the basis of: the surveillance area size, the peculiarities of the sought target, the quality of the used sensors, etc.
In Subsection 3.2 a tracking algorithm which takes advantage of the above multistatic system is introduced. In addition, such an algorithm relies on the main idea behind the TBD paradigm, namely, it jointly processes the available measurements over several consecutive pings.

3. Target tracking: the track-before-detect approach

Traditional tracking algorithms are designed assuming that the sensor provides a set of discrete measurements at each scan (or ping). In an activated surveillance system such measurements could be obtained by thresholding the output of a matched filter fed by a baseband version of collected data. Then, the tracking algorithm links measurements across time and estimates the parameters of interest. The threshold value must be low enough to guarantee a sufficiently high probability of target detection. However, a low threshold gives rise to a high rate of false alarms. It follows that to avoid false tracks it is necessary to effectively solve the data association problem (Bar-Shalom & Fortmann, Academic Press 1988). A reliable means of validating the track estimate as a target-originated one is also required.
An alternative approach, referred to as track-before-detect (TBD), consists of feeding the processor with unthresholded data or thresholded data with significantly lower thresholds than the ones used by conventional trackers. TBD-based procedures jointly process several consecutive pings (or scans) and, relying on a target kinematics or, simply, exploiting the

physically admissible target transitions, jointly declare the presence of a target and, eventually, its track. A TBD algorithm can improve track accuracy and follow low SNR targets at the price of an increase of the computational complexity. Moreover, a TBD scheme ensuring the constant false alarm rate property with respect to the unknown statistics of the disturbance controls the overall false track acceptance probability and, hence, it is capable of guaranteeing the constant false track acceptance rate (CFTAR property).

Most of the TBD algorithms existing in the open literature are conceived to be implemented in optical and radar systems. Their use in connection with sonar systems has received less attention. For a description of existing results see (Orlando et al., IEEE-TSP 2010; Buzzi et al., IEEE-TAES 2005; S. Buzzi et al., IEEE-TAES 2008; Kramer & Reid, Radar Conference 1990; Wallace, Radar Conference 2002). A family of low-complexity power-efficient TBD procedures has been presented in (Buzzi et al., IEEE-TAES 2005). Therein, the continuous-time continuous-amplitude signal collected by a pulse Doppler radar is discretized to reflect the sectorization of the coverage area and the range gating operation, and the generalized likelihood ratio test (GLRT) is solved resorting to a Viterbi-like tracking algorithm. The proposed algorithm has a complexity linear in the number of integrated scans and in the time on target. The emphasis is on detection performance more than tracking: in fact, the GLRT does not rely on the target kinematics; it simply takes into account a maximum target velocity in order to define the admissible target transitions in range and azimuth (the Doppler is dealt with as a nuisance quantity due to the considered system and target parameters). However, a rough estimate of the target parameters is obtained as a by-product of the construction of the target statistic. (Orlando et al., IEEE-TSP 2010) extends the derivation of (Buzzi et al., IEEE-TAES 2005) to the context of space-time adaptive processing.

In the next subsection, we focus on a bistatic architecture and describe a proper modification of the algorithms proposed in (Orlando et al., IEEE-TSP 2010) to handle raw hydrophone data. In Subsection 3.2 we apply the main idea behind the TBD approach to thresholded data provided by a sensor network over several consecutive pings.

3.1 Track-before-detect strategies for bistatic sonars

The system considered here has a bistatic configuration and integrates the returns from M consecutive pings before deciding whether or not a target is present in the surveillance area. Relying on the mathematical model for the received signal derived in Subsection 2.1.1, we utilize design criteria based upon the GLRT to derive a class of adaptive detectors which guarantee the CFTAR property under design assumptions with respect to the overall spectral properties of the noise. Moreover, at the design stage, we assume that the unknown clutter covariance matrix can possibly change from ping to ping. The performance assessment is provided in Section 5. It is carried out resorting to real sonar data collected by the deployable underwater surveillance system, called DEMUS, of NATO Undersea Research Centre (NURC).

3.1.1 Detector designs

As stated above, the receiver jointly processes data from M consecutive pings before discriminating between the noise-only hypothesis and the signal-plus-noise hypothesis. Thus, the track-before-detect problem at hand can be formulated in terms of a binary hypothesis

testing problem as follows (Orlando et al., IEEE-TSP 2010)

$$\begin{cases} H_0 : \boldsymbol{z}_{l,m} = \boldsymbol{n}_{l,m}, & l = 1,\ldots,L, \quad m = 1,\ldots,M \\ H_1 : \begin{cases} \boldsymbol{z}_{l,m} = \alpha_m \boldsymbol{v}(\theta_{r,m}) + \boldsymbol{n}_{l,m}, & l = l_m, \quad m = 1,\ldots,M, \\ \boldsymbol{z}_{l,m} = \boldsymbol{n}_{l,m}, & l \neq l_m, \quad m = 1,\ldots,M, \end{cases} \end{cases} \tag{39}$$

where

- $l \in \{1,\ldots,L\}$ and $m \in \{1,\ldots,M\}$ are integers indexing the range cells and the pings, respectively;
- $\boldsymbol{z}_{l,m} \in \mathbb{C}^{N\times 1}$, $l = 1,\ldots,L$, $m = 1,\ldots,M$, are the vectors containing the noisy returns;
- $\boldsymbol{n}_{l,m} \in \mathbb{C}^{N\times 1}$, $l = 1,\ldots,L$, $m = 1,\ldots,M$, are independent and identically distributed complex normal random vectors with zero mean and unknown covariance matrices $\boldsymbol{R}_m \in \mathbb{C}^{N\times N}$;
- $\theta_{r,m}$ denotes the azimuthal angle of the impinging target echo at the mth ping.

The above assumptions imply that the probability density function (pdf) of the overall data matrix, denoted by

$$\boldsymbol{Z} = [z_{1,1} \ \cdots \ z_{L,M}], \tag{40}$$

can be written as

$$f_0(\boldsymbol{Z}; \boldsymbol{R}_1,\ldots,\boldsymbol{R}_M) = \prod_{m=1}^{M} \frac{1}{\pi^{NL}\det(\boldsymbol{R}_m)^L} \exp\left\{-\mathrm{Tr}\left[\boldsymbol{R}_m^{-1}\left(\boldsymbol{z}_{l_m,m}\boldsymbol{z}_{l_m,m}^{\dagger} + \boldsymbol{S}_{l_m,m}\right)\right]\right\} \tag{41}$$

under H_0 and

$$f_1(\boldsymbol{Z}; \boldsymbol{R}_1,\ldots,\boldsymbol{R}_M, \boldsymbol{\alpha}) = \prod_{m=1}^{M} \frac{1}{\pi^{NL}\det(\boldsymbol{R}_m)^L} \exp\left\{-\mathrm{Tr}\left[\boldsymbol{R}_m^{-1}\left(\boldsymbol{u}_{l_m,m}\boldsymbol{u}_{l_m,m}^{\dagger} + \boldsymbol{S}_{l_m,m}\right)\right]\right\} \tag{42}$$

under H_1, where

- $\det(\cdot)$ and $\mathrm{Tr}[\cdot]$ denote the determinant and the trace of a square matrix, respectively;
- $\boldsymbol{S}_{l_m,m} \in \mathbb{C}^{N\times N}$ is $(L-1)$ times the sample covariance matrix of the noise based on the available data over the mth ping, but for the l_mth range cell, namely

$$\boldsymbol{S}_{l_m,m} = \sum_{l\neq l_m} \boldsymbol{z}_{l,m}\boldsymbol{z}_{l,m}^{\dagger}; \tag{43}$$

- $\boldsymbol{\alpha} = [\alpha_1 \ \cdots \ \alpha_M]^T$ is the vector of target responses and[6]

$$\boldsymbol{u}_{l_m,m} = \boldsymbol{z}_{l_m,m} - \alpha_m \boldsymbol{v}_m(\theta_{r,m}). \tag{44}$$

In the following we apply the so-called two-step GLRT-based design procedure (Kelly & Nitzberg, IEEE-TAES 1992) in order to come up with a class of fully-adaptive detectors. To be more precise, the following rationale is adopted

- first assume that the covariance matrices of the noise are known $\forall m$ and implement the GLRT maximizing the likelihood functions over the unknown parameters;

[6] Recall that $\boldsymbol{v}_m$ is defined by (32)

- then, replace the unknown matrices $\boldsymbol{R}_m$, $m = 1, \ldots, M$, with proper estimates.

Thus, the GLRT under the assumption that the $\boldsymbol{R}_m$'s are known is given by

$$\frac{\max\limits_{\boldsymbol{\mathcal{D}} \in \mathcal{S}} \max\limits_{\boldsymbol{\alpha}} f_1(\boldsymbol{Z}; \boldsymbol{\mathcal{D}}, \boldsymbol{\alpha}, \boldsymbol{R}_1, \ldots, \boldsymbol{R}_M)}{f_0(\boldsymbol{Z}; \boldsymbol{R}_1, \ldots, \boldsymbol{R}_M)} \underset{H_0}{\overset{H_1}{\gtrless}} \eta, \tag{45}$$

where

- $\boldsymbol{\mathcal{D}} = \{(l_1, \theta_{r,1}), \ldots, (l_M, \theta_{r,M})\} \in \mathcal{S}$ is the sequence of points occupied by a prospective target in the Range-Azimuth domain, with $\mathcal{S}$ the set of all physically admissible target trajectories;
- η is the threshold value to be set in order to ensure the desired probability of false alarm (P_{fa}).

Performing the maximization of (45) with respect to $\boldsymbol{\alpha}$ yields

$$\max_{\boldsymbol{\mathcal{D}} \in \mathcal{S}} \sum_{m=1}^{M} \frac{\left| \boldsymbol{v}(\theta_{r,m})^\dagger \boldsymbol{R}_m^{-1} \boldsymbol{z}_{l_m,m} \right|^2}{\boldsymbol{v}(\theta_{r,m})^\dagger \boldsymbol{R}_m^{-1} \boldsymbol{v}(\theta_{r,m})} \underset{H_0}{\overset{H_1}{\gtrless}} \eta. \tag{46}$$

An adaptive version of decision scheme (46) can be obtained by replacing the $\boldsymbol{R}_m$'s with proper estimates, $\widehat{\boldsymbol{R}}_m$'s say. The most common estimate of $\boldsymbol{R}_m$ is the sample covariance matrix based upon the available data at the mth ping, namely

$$\widehat{\boldsymbol{R}}_m = \frac{1}{L} \sum_{l=1}^{L} \boldsymbol{z}_{l,m} \boldsymbol{z}_{l,m}^\dagger. \tag{47}$$

The above estimate can be alternatively modified in order to exclude range cells contaminated by useful echoes as follows

$$\widehat{\boldsymbol{R}}_m = \frac{1}{K} \sum_{l \in \Omega_R \setminus \Omega_T} \boldsymbol{z}_{l,m} \boldsymbol{z}_{l,m}^\dagger, \tag{48}$$

where

- $\Omega_R = \{1, \ldots, L\}$;
- Ω_T is the set of consecutive integers indexing the range cells contaminated by target returns;
- K is the cardinality of $\Omega_R \setminus \Omega_T$, namely the set containing the elements of Ω_R that do not belong to Ω_T.

3.1.2 Implementation issues

This subsection is aimed at discussing some implementation issues concerning the above TBD algorithm. In fact, an adaptive version of (46) is time consuming since it requires maximization with respect to the sequence $\boldsymbol{\mathcal{D}}$ of pairs $(l_m, \theta_{r,m})$. In order to overcome this limitation, observe that maximization over $\boldsymbol{\mathcal{D}}$ cannot be conducted separately with respect to the $(l_m, \theta_{r,m})$ pairs: indeed, physical constraints on the target trajectory imply that $(l_{m+1}, \theta_{r,m+1})$ depends upon

$$\{(l_1, \theta_{r,1}), \ldots, (l_m, \theta_{r,m})\}, \quad m = 1, \ldots, M-1. \tag{49}$$

Moreover, let us partition the azimuth region as follows

$$\Omega_A = \left\{ \frac{1}{q} 2\pi, \frac{2}{q} 2\pi, \ldots, 2\pi \right\}, \tag{50}$$

where $q \in \mathbb{N}$ is a parameter which controls the accuracy of the azimuthal angle estimate. With these simplifications in mind, it is possible to recast detector (46) as follows

$$\max_{\substack{\boldsymbol{\mathcal{D}} \in (\Omega_R \times \Omega_A)^M \\ (l_m, \theta_{r,m}) \in \mathcal{P}((l_{m-1}, \theta_{r,m-1}))}} \sum_{m=1}^{M} \frac{\left| \boldsymbol{v}_m(\theta_{r,m})^\dagger \boldsymbol{R}_m^{-1} \boldsymbol{z}_{l_m,m} \right|^2}{\boldsymbol{v}_m(\theta_{r,m})^\dagger \boldsymbol{R}_m^{-1} \boldsymbol{v}_m(\theta_{r,m})} \underset{H_0}{\overset{H_1}{\gtrless}} \eta, \tag{51}$$

where

- $\times$ denotes the Cartesian product;
- $(\Omega_R \times \Omega_A)^M$ is the Mth Cartesian power of the set $(\Omega_R \times \Omega_A)$;
- $\mathcal{P}((l_{m-1}, \theta_{r,m-1}))$ denotes the set of elements of $(\Omega_R \times \Omega_A)$ that can be reached from $(l_{m-1}, \theta_{r,m-1})$ under the upper bounds V_R and V_A on the radial velocity and on the tangential velocity of the target, respectively.

The above optimization problem can be solved constructing an expanded trellis diagram, whose states are the elements of $\Omega_R \times \Omega_A$ and hence using a Viterbi-like procedure to find the best path metric in this expanded trellis (Buzzi et al., IEEE-TAES 2005; Forney, IEEE Proc. 1973). The Viterbi algorithm would require determining (at most) Lq paths in the expanded trellis diagram of depth M, with a consequent maximum complexity[7] $\mathcal{O}(LqM)$ (linear in the number of ping). Finally, it is easy to prove that (51) coupled with (47) or (48) ensures the CFTAR property with respect to the unknown noise parameters.

3.2 A batch tracking algorithm for multistatic sonars

In this subsection, a tracking algorithm for multistatic sonars is derived, that borrows the main idea of the TBD approach by jointly processing thresholded data over several consecutive pings. The considered system is described in Subsection 2.2. In order to estimate the target trajectory, the likelihood function of the measurements (that depends on the target position at each ping) is maximized by resorting to a Viterbi-like procedure (see Subsection 3.1). For the reader's ease, recall that

$$Z_{i,m} = \{ \boldsymbol{z}_{i,1,m}, \ldots, \boldsymbol{z}_{i,N_{i,m},m} \} \tag{52}$$

denotes the set of measurements transmitted to the fusion center by the ith receiver at the mth ping, where

$$\boldsymbol{z}_{i,j,m} = \begin{bmatrix} d_{i,j,m} \\ \phi_{i,j,m} \end{bmatrix} \tag{53}$$

with $d_{i,j,m}$ the TDOA and $\phi_{i,j,m}$ the bearing. In the following, we assume the presence of one maneuvering target with deterministic motion in the surveillance region.
Let us start denoting by

$$Z = \{ Z_{1,1}, \ldots, Z_{1,M}, \ldots, Z_{N_r,1}, \ldots, Z_{N_r,M} \} \tag{54}$$

[7] We resort to the usual Landau notation.

the overall data set and defining a grid G of $N_x N_y$ points[8], that covers the entire surveillance region. At the mth ping the nominal position of the target is given by

$$\boldsymbol{x}_m = \begin{bmatrix} x_m \\ y_m \end{bmatrix}, \quad (x_m, y_m) \in G. \tag{55}$$

Now, assuming that, given the sequence of the nominal target positions over M consecutive pings, denoted by

$$X = \{\boldsymbol{x}_1, \boldsymbol{x}_2, \ldots, \boldsymbol{x}_M\}, \tag{56}$$

the measurements are independent of each other, it is not difficult to show that the pdf of Z can be written as follows

$$f_1(Z; X, J) = \prod_{m=1}^{M} \prod_{i=1}^{N_r} \left\{ \frac{(1 - P_{i,m})}{(U_{i,m})^{N_{i,m}}} + P_{i,m} \frac{f_z(\boldsymbol{z}_{i,j_{i,m},m}; \boldsymbol{x}_m)}{(U_{i,m})^{N_{i,m}-1}} \right\}, \tag{57}$$

where $P_{i,m}$ is the probability of detection of the ith receiver at the mth ping[9], $j_{i,m} \in \mathbb{N}$ is an integer indexing the target originated contact for the ith receiver at the mth ping,

$$J = \{J_1, \ldots, J_M\}, \quad \text{with} \quad J_m = \{j_{1,m}, \ldots, j_{N_r,m}\}, \tag{58}$$

$$U_{i,m} = (d_{i,m}^{\max} - d_{i,m}^{\min})(\phi_{i,m}^{\max} - \phi_{i,m}^{\min}). \tag{59}$$

Finally, $f_z(\cdot;\cdot)$ is given by

$$f_z(\boldsymbol{z}_{i,j_{i,m},m}; \boldsymbol{x}_m) = \frac{1}{2\pi[\det(\boldsymbol{R})]^{1/2}} \times \exp\left\{ -\frac{1}{2} \left(\boldsymbol{z}_{i,j_{i,m},m} - \boldsymbol{\zeta}(\boldsymbol{x}_m, \boldsymbol{r}_i, \boldsymbol{s}_{n_{sr}}) \right)^T \boldsymbol{R}^{-1} \left(\boldsymbol{z}_{i,j_{i,m},m} - \boldsymbol{\zeta}(\boldsymbol{x}_m, \boldsymbol{r}_i, \boldsymbol{s}_{n_{sr}}) \right) \right\}, \tag{60}$$

where

$$\boldsymbol{R} = \begin{bmatrix} \sigma_d^2 & 0 \\ 0 & \sigma_\theta^2 \end{bmatrix}, \quad \boldsymbol{r}_i = \begin{bmatrix} r_{x,i} \\ r_{y,i} \end{bmatrix} \in \mathbb{R}^{2\times 1}, \quad \text{and} \quad \boldsymbol{s}_{n_{sr}} = \begin{bmatrix} s_{x,n_{sr}} \\ s_{y,n_{sr}} \end{bmatrix} \in \mathbb{R}^{2\times 1} \tag{61}$$

are the covariance matrix of $\boldsymbol{z}_{i,j_{i,m},m}$, the position of the ith receiver, and the position of the n_{sr}th source[10], respectively, and $\boldsymbol{\zeta}(\cdot,\cdot,\cdot)$ is a vector valued function such that

$$\boldsymbol{\zeta}(\boldsymbol{x}_m, \boldsymbol{r}_i, \boldsymbol{s}_{n_{sr}}) = \begin{bmatrix} \frac{1}{c}\left(\|\boldsymbol{s}_{n_{sr}} - \boldsymbol{x}_m\| + \|\boldsymbol{x}_m - \boldsymbol{r}_i\| - \|\boldsymbol{r}_i - \boldsymbol{s}_{n_{sr}}\| \right) \\ \frac{\pi}{2} + \pi(1 - u(x)) - \tan^{-1} \dfrac{(y_m - r_{y,i})}{(x_m - r_{x,i})} \end{bmatrix}, \tag{62}$$

where[11] $u(\cdot)$ is a step function taking value 1 over the interval $[0 \ +\infty[$. In other words, $\boldsymbol{\zeta}(\cdot,\cdot,\cdot)$ converts coordinates (x_m, y_m) into the corresponding values of TDOA and bearing with respect to the ith receiver and the n_{sr}th source.

[8] $N_x, N_y \in \mathbb{N}$
[9] The $P_{i,m}$'s are assumed known.
[10] n_{sr} is given by equation (34).
[11] Recall that $\|\cdot\|$ denotes the Euclidean norm of a vector and c is the sound propagation velocity.

Dividing equation (57) by the pdf of Z under the noise-only hypothesis, given by

$$f_0(Z) = \prod_{m=1}^{M} \prod_{i=1}^{N_r} \frac{1}{U_{i,m}^{N_{i,m}}}, \tag{63}$$

we obtain the likelihood ratio

$$\Lambda(Z; X, J) = \prod_{m=1}^{M} \prod_{i=1}^{N_r} \left\{ (1 - P_{i,m}) + P_{i,m} f(\boldsymbol{z}_{i,j_{i,m},m}; \boldsymbol{x}_m) U_{i,m} \right\}, \tag{64}$$

which, by taking the logarithm, becomes

$$\Lambda(Z; X, J) = \sum_{m=1}^{M} \sum_{i=1}^{N_r} \log \left\{ (1 - P_{i,m}) + P_{i,m} f(\boldsymbol{z}_{i,j_{i,m},m}; \boldsymbol{x}_m) U_{i,m} \right\}. \tag{65}$$

Observe that the likelihood ratio (65) is a function of the target state sequence X and of the target originated measurement indexes J, which are unknown and, consequently, have to be estimated. To this end, the likelihood ratio (65) is maximized with respect to X and J. The optimization with respect to j_m, $m = 1, \ldots, M$, is straightforward and solves the data association problem; in fact, given the ping index m and the target state $\boldsymbol{x}_m$, for each receiver it is possible to select that measurement index[12], $\widehat{j}_{i,m}$ say, which minimizes the following Mahalanobis distance

$$\widehat{j}_{i,m} = \arg \min_{j_{i,m} \in J_m} \left(\boldsymbol{z}_{i,j_{i,m},m} - \boldsymbol{\zeta}(\boldsymbol{x}_m, \boldsymbol{r}_i, \boldsymbol{s}_{n_{sr}}) \right)^T \boldsymbol{R}^{-1} \left(\boldsymbol{z}_{i,j_{i,m},m} - \boldsymbol{\zeta}(\boldsymbol{x}_m, \boldsymbol{r}_i, \boldsymbol{s}_{n_{sr}}) \right). \tag{66}$$

It follows that (65) can be recast as

$$\Lambda(Z; X, \widehat{J}) = \sum_{m=1}^{M} \sum_{i=1}^{N_r} \log \left\{ (1 - P_{i,m}) + P_{i,m} f(\boldsymbol{z}_{i,\widehat{j}_{i,m},m}; \boldsymbol{x}_m) U_{i,m} \right\}, \tag{67}$$

where

$$\widehat{J} = \left\{ \widehat{J}_1, \ldots, \widehat{J}_M \right\} \quad \text{with} \quad \widehat{J}_m = \left\{ \widehat{j}_{1,m}, \ldots, \widehat{j}_{N_r,m} \right\}. \tag{68}$$

Finally, in order to estimate the sequence of target positions, it is worth taking into consideration physical constraints on the target trajectory, that limit the maximum number of point transitions throughout G between two consecutive pings. With this assumption in mind, an estimate of X can be obtained as follows

$$\begin{aligned} \widehat{X} = \arg\max_{X} \Lambda(Z; X, \widehat{J}), \\ \boldsymbol{x}_m \in \mathcal{P}(\boldsymbol{x}_{m-1}) \end{aligned} \tag{69}$$

where $\mathcal{P}(\boldsymbol{x}_{m-1})$ denotes the set of target states that can be reached from $\boldsymbol{x}_{m-1}$ under an upper bound on the target velocity. The above optimization problem can be solved by resorting to a Viterbi-like procedure to find the best path metrics in an expanded trellis diagram of depth M whose states are the points of G (see Figures 3). In Section 5 some illustrative examples show the effectiveness of the above approach.

[12] Recall that the J_m's are finite discrete sets.

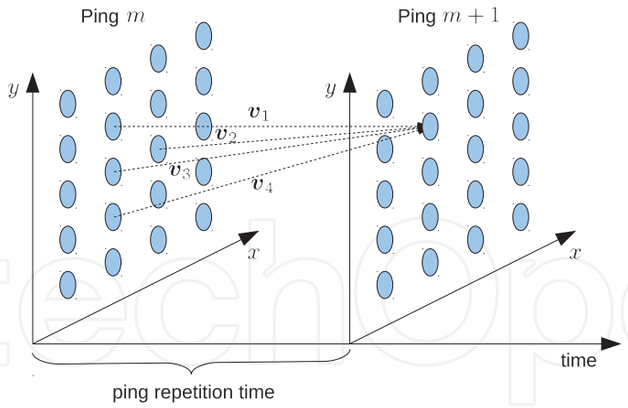

Fig. 3. The expanded trellis whose states are the points of G.

4. Sensor selection strategies for multistatic sonars

This section describes on a conceptual level a method to select those sensors whose measurements will be fed to the batch algorithm presented in Subsection 3.2. Consider the sensor network described in Subsection 2.2 and assume that SNR measurements, $\mathrm{SNR}_{i,j,m}$ say, are also available at the fusion center. The statistical distribution of the SNR measurements is assigned as follows

$$\mathrm{SNR}_{i,j,m} \sim \mathcal{N}_1(\mu_{i,m}, \sigma^2_{\mathrm{SNR}}), \tag{70}$$

$$i = 1, \ldots, N_r, \quad j = 1, \ldots, N_{i,m}, \quad m = 1, \ldots, M, \tag{71}$$

where $\sigma_{\mathrm{SNR}} > 0$ is the standard deviation and (Urick, McGraw-Hill 1983)

$$\mu_{i,m} = \begin{cases} \mathrm{SL} + \mathrm{TL}^{\mathrm{ST}}_m + \mathrm{TL}^{\mathrm{TR}}_{i,m} + \mathrm{TS}(\psi_{i,m}), & \text{if the contact is originated from the target,} \\ \gamma_{i,m}, & \text{otherwise.} \end{cases} \tag{72}$$

In (72), $\gamma_{i,m} \in \mathbb{R}$, SL is the source level, $\mathrm{TL}^{\mathrm{ST}}_m$ is the transmission loss between the n_{sr}th source, with n_{sr} given by (34), and the target, $\mathrm{TL}^{\mathrm{TR}}_{i,m}$ is the transmission loss between the target and the ith receiver, and $\mathrm{TS}(\psi_{i,m})$ is the target strength which depends on the aspect angle of the target, $\psi_{i,m}$ say, with respect to the ith receiver. The transmission loss $\mathrm{TL}^{\mathrm{AB}}$ between two points A and B spaced D meters apart from one another is defined as follows (Urick, McGraw-Hill 1983)

$$\mathrm{TL}^{\mathrm{AB}} = \begin{cases} 10\log_{10}\left(\dfrac{1}{D^2}\right), & \text{in case of spherical spreading of the sound wave,} \\ 10\log_{10}\left(\dfrac{1}{D}\right), & \text{in case of cylindrical spreading of the sound wave.} \end{cases} \tag{73}$$

The likelihood function of the SNR for the ith receiver at the mth ping can be written as follows

$$f^{i,m}_{\mathrm{SNR}}(\alpha_{i,m}; j_{i,m}, \psi_{i,m}) = \frac{(1 - P_{i,m})}{(\sqrt{2\pi}\sigma_{\mathrm{SNR}})^{N_{i,m}}} \exp\left\{ -\frac{1}{2\sigma^2_{\mathrm{SNR}}} \sum_{k=1}^{N_{i,m}} (\mathrm{SNR}_{i,k,m} - \gamma_{i,m})^2 \right\}$$

$$+ P_{i,m} \frac{\exp\left\{ -\dfrac{1}{2\sigma^2_{\mathrm{SNR}}} \left[\displaystyle\sum_{k=1, k\neq j_{i,m}}^{N_{i,m}} (\mathrm{SNR}_{i,k,m} - \gamma_{i,m})^2 + (\mathrm{SNR}_{i,j_{i,m},m} - \mathrm{C} - \mathrm{TS}(\psi_{i,m}))^2 \right] \right\}}{(\sqrt{2\pi}\sigma_{\mathrm{SNR}})^{N_{i,m}}}, \tag{74}$$

where

- $\alpha_{i,m} = \left\{\mathrm{SNR}_{i,1,m}, \mathrm{SNR}_{i,2,m}, \ldots, \mathrm{SNR}_{i,N_{i,m},m}\right\}$;
- $j_{i,m} \in \{1, \ldots, N_{i,m}\}$ is the index of the target-originated measurement;
- $\mathrm{C} = \mathrm{SL} + \mathrm{TL}_m^{\mathrm{ST}} + \mathrm{TL}_{i,m}^{\mathrm{TR}}$.

In (74), $j_{i,m}$ and $\psi_{i,m}$ are not known and have to be estimated from the observables. To this end $f_{\mathrm{SNR}}^{i,m}(\cdot;\cdot,\cdot)$ is maximized with respect to such parameters. More specifically, observe that

$$\widehat{\psi}_{i,m} = \arg \max_{\psi_{i,m} \in [0,\, 360)} f_{\mathrm{SNR}}^{i,m}(\alpha_{i,m}; j_{i,m}, \psi_{i,m}) = \arg \max_{\psi_{i,m} \in [0,\, 360)} \mathrm{TS}(\psi_{i,m}) \tag{75}$$

and that maximization over $j_{i,m}$ can be performed in the same manner as pointed out for (66). Next, we arrange the likelihood functions at the mth ping in ascending order, namely

$$f_{\mathrm{SNR}}^{i_{1,m},m} < f_{\mathrm{SNR}}^{i_{2,m},m} < \ldots < f_{\mathrm{SNR}}^{i_{N_r,m},m} \tag{76}$$

and select the last K to form the following set of indexes[13]

$$S_m = \{i_{N_r-K+1,m}, i_{N_r-K+2,m}, \ldots, i_{N_r,m}\}. \tag{77}$$

Once sensors have been selected, the target trajectory can be estimated as follows

$$\widehat{X} = \arg \max_{\substack{X \\ \boldsymbol{x}_m \in \mathcal{P}(\boldsymbol{x}_{m-1})}} \left[\max_{J} \Lambda_1(Z; X, J)\right], \tag{78}$$

where

$$\Lambda_1(Z; X, J) = \sum_{m=1}^{M} \sum_{i \in S_m} \log\left\{(1 - P_{i,m}) + P_{i,m} f(\boldsymbol{z}_{i,j_{i,m},m}; \boldsymbol{x}_m) U_{i,m}\right\}. \tag{79}$$

Observe that (78) is less time-demanding than (69) since the maximizations over J and X are performed processing data from $K < N_r$ receivers.

5. Illustrative examples and discussion

5.1 Track-before-detect approach for raw data

The TBD approach described in Subsection 3.1 leads to a class of algorithms capable of handling raw hydrophone data. This subsection is aimed at proving the feasibility and the effectiveness of such algorithms using experimental bistatic sonar data collected by the NURC's DEMUS sensor array in the course of PreDEMUS'06 sea trial.

The setup of PreDEMUS'06 is shown in Figure 4 and involves a transmitter, three receivers and as target a towed sound source, called echo-repeater (E-R). The E-R, towed by a surface vessel at a depth of 80 m, retransmits received source signals with a specified amplification and a certain delay. The source transmits a frequency-modulated pulse waveform of duration $T_p = 1$ sec, bandwidth $B = 100$ Hz, and carrier frequency $f_c = 2500$ Hz. The resulting range resolution is about 7 m (we are assuming that $c = 1500$ m/sec). The receiver is a planar array (as shown in Figure 1) with $N_a = 9$ arms, $N_s = 8$ sensors, $\theta_a = 40$ degrees, and $d = 0.289$ m. The total number of sensors is $N = 64$ (remember that the arms share the central sensor).

[13] K may be chosen according to a preassigned criterion.

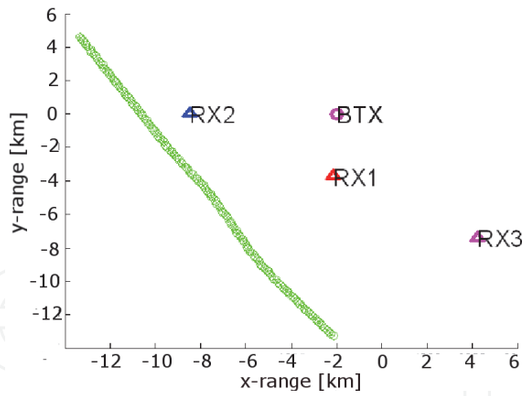

Fig. 4. PreDEMUS'06 setup. The fuchsia circle represents the transmitter, the red triangle represents the receiver 1, the blue triangle represents the receiver 2, finally the fuchsia triangle represents the receiver 3. The sequence of green circles is the target trajectory. [Courtesy M. Daun]

In the sequel, we examine the behavior of the receiver (51) only coupled with (48), where Ω_T is appropriately selected. Moreover, we consider a scenario where the useful signal echoes are strong enough to guarantee a good number of contacts for traditional tracking systems (strong-target scenario) and a scenario where the detection performance of the envelope detector is poor (weak-target scenario). The algorithm processes data corresponding to a little patch of the surveillance area and the target is moving within such a patch throughout the entire observation time. The processed patch takes up a region of about 2 seconds in range and at most 35 degrees in azimuth[14]. As to the threshold, it is set in order to have no detection when the algorithm is fed by noise-only data.
In Figures 5a-5c, we show the performance of the proposed algorithm in terms of target position estimate when it operates in the first scenario (for more details on the data set see Figure 4 of (Daun & Ehlers, JASP 2010)); more precisely, we process data from receiver 1 and pings 91-99 (scenario A1) in Fig. 5a, from receiver 2 and pings 76-84 (scenario A2) in Fig. 5b, and from receiver 3 and pings 100-108 (scenario A3) in Fig. 5c. The figures also report the trajectory of the E-R which is taken as reference. Observe that in this case the estimated target locations, represented by the line markers, closely follow the reference track. Observe that the estimated tracks exhibit some "fluctuations". This is partly due to the fact that estimation errors also depend on the undercurrent which modifies the receiver orientation (heading) and, consequently, introduces an additional uncertainty in the azimuth estimation. Otherwise stated, the position of the reference arm of each receiver is time-varying. Such heading errors can be partly compensated by using data recorded from an on-board compass. In Figure 5d, we plot the estimated target positions returned by the algorithm in the case of a low observable target; in particular, we consider data from receiver 1 and pings 16-26 (scenario B1). The figure highlights two important aspects of the TBD approach. First, the proposed algorithm can detect a low SNR target, whereas the envelope detectors, used by conventional tracking systems, are completely blind (Daun & Ehlers, JASP 2010). Second, it provides, as a by product, a rough estimate of the target locations. Notice that also in this figure, the heading errors make the curve representing the estimated trajectory "convoluted".

[14] A preliminary statistical analysis highlights that such data exhibit a "good" level of homogeneity.

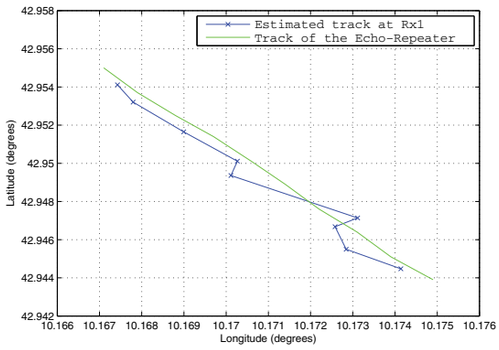

(a) Scenario A1 assuming $M = 9$ and $K > 2N$.

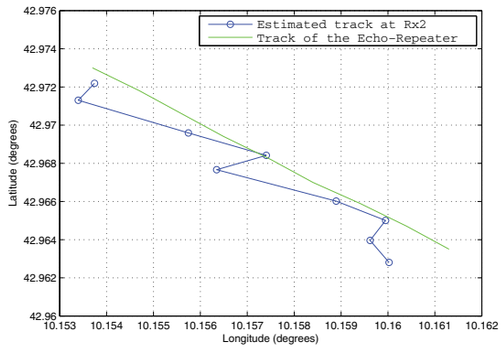

(b) Scenario A2 assuming $M = 9$ and $K > 2N$.

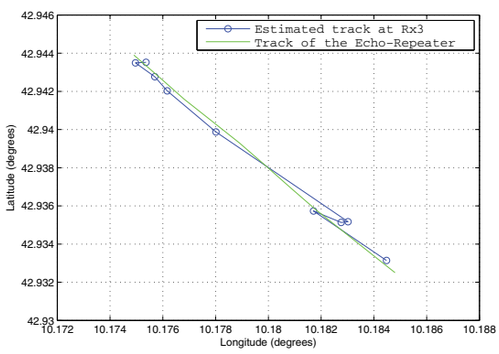

(c) Scenario A3 assuming $M = 9$ and $K > 2N$.

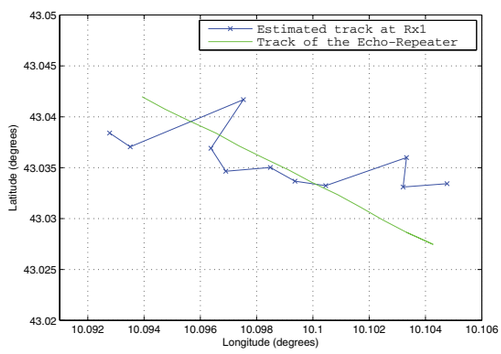

(d) Scenario B1 assuming $M = 11$ and $K > 2N$.

Fig. 5. Estimated target locations for scenarios A1, A2, A3, and B1.

As a final remark, the estimation of the $\boldsymbol{R}_m$'s can be automated modifying detector (51) as follows (Bandiera et al., IEEE-SPL 2006)

$$\max_{\Omega_T} \max_{\substack{\boldsymbol{\mathcal{D}} \in (\Omega_R \times \Omega_A)^M \\ (l_m, \theta_{r,m}) \in \mathcal{P}((l_{m-1}, \theta_{r,m-1}))}} \sum_{m=1}^{M} \frac{|\boldsymbol{v}_m(\theta_{r,m})^\dagger \widehat{\boldsymbol{R}}_m^{-1} \boldsymbol{z}_{l_m,m}|^2}{\boldsymbol{v}_m(\theta_{r,m})^\dagger \widehat{\boldsymbol{R}}_m^{-1} \boldsymbol{v}_m(\theta_{r,m})} \underset{H_0}{\overset{H_1}{\gtrless}} \gamma, \tag{80}$$

where again $\widehat{\boldsymbol{R}}_m$ is given by (48).

5.2 Contact-based maximum-likelihood tracker

The subsection contains some illustrative examples to show the tracking performance of the contact-based tracker introduced in Subsection 3.2. Two different scenarios are considered.

5.2.1 Test scenario 1

Consider $N_r = 12$ hydrophones (Rx) and $N_{sr} = 4$ sources (Sr) placed in the positions listed in Table 1. Moreover, we assume $P_{i,m} = P_d$, $\forall i, m$. The surveillance region is a 16740×16740 m^2 square with the upper left corner at $(37500, 34500)$ m and it is covered by a grid of 31×31 points 540 m spaced apart. Such a separation corresponds to a nominal target velocity of 6 knots. The total number of processed ping is $M = 20$ and the time interval between consecutive pings is $T_{pg} = 180$ seconds. As to the synthetic target, we assume that it moves

within the surveillance area with a constant velocity of about 6 knots and that after 10 pings its direction of motion changes and becomes orthogonal to the previous direction.
The standard deviations of target originated measurements are set as follows

$$\sigma_d = 0.4 \text{ sec} \quad \text{and} \quad \sigma_\phi = 8 \text{ degrees}, \tag{81}$$

while for each couple source-receiver the false contacts are distributed uniformly in the bistatic ellipse that contains the surveillance region.
Finally, the number of false contacts, namely those not originated from the target, obeys to the Poisson distribution with parameter

$$\lambda = P_{fa} N_{\text{cell}}, \tag{82}$$

where P_{fa} is the probability of false alarm in any cell and N_{cell} is the total number of cells. All simulation results assume $P_{fa} = 0.01$ and $\lambda = 9.6$.
In Figures 6a-6c we show the estimated tracks from 4 independent trials. Each figure refers to different values of P_d and reports the actual trajectory of the target (ground truth). Observe that for low values of P_d ($P_d = 0.3$) the proposed algorithm is still capable of providing an estimate of the target positions, even though the estimation error is significant. On the other hand, for greater values of P_d the estimated target locations closely follow the ground truth. Such results are confirmed by Figure 6d, where we plot the root mean square (RMS) values based on 300 independent trials versus the P_d.

5.2.2 Test scenario 2 (from the multistatic tracking working group)

The intent of the multistatic tracking working group (MSTWG) is to foster the exchange of scientific and technical ideas, problems, and solutions related to multistatic tracking for sonar and radar. This includes the collaborative analysis of common data sets and culminate in workshops or special sessions disseminating the results. The MSTWG was founded as an ad hoc working group in December 2004, with a three year charter. In July 2007, based on mutual agreement between the International Society of Information Fusion (ISIF) board of directors and the current group membership, it was agreed to formalize the MSTWG as a working group under the auspices of ISIF. The objective of the ISIF MSTWG is to promote collaboration among its members in multisensor fusion and tracking, with a current focus on multistatic sonar and radar. This collaboration is achieved through regular meetings, participation in special sessions at conferences, and the analysis of common data sets. One of these data sets is

Rx number	**X (meters)**	**Y (meters)**	**Rx number**	**X (meters)**	**Y (meters)**
1	26752,91	8219,99	10	36033,99	36000
2	26752,91	26740	11	54581,52	17479,99
3	26752,91	45259,99	12	54581,52	36000
4	45285,83	8219,99	**Sr number**	**X (meters)**	**Y (meters)**
5	45285,83	45259,99	1	17486.46	54520
6	63818,75	8219,99	2	54581,52	17480
7	63818,75	26740	3	54581,52	54520
8	63818,75	45259,99	4	17486.46	17480
9	36033,99	17479,99			

Table 1. Sensor coordinates.

the Metron data set (Orlov, Metron Data set 2009). In the following a brief description of the data set is given (further details can be found in (Orlov, Metron Data set 2009)).
The operational field is a 72000×72000 m^2 square with the origin at $(0, 0)$ m. The sensors are laid out as two concentric square grids centered about $(x, y) = (36000, 36000)$ m. All sensors are stationary. The first grid consists of 16 sensors, laid out 4×4 beginning at $(x, y) = (8220, 8220)$ m, with four receivers within a row 18520 m apart horizontally and four rows 18520 m apart vertically. All of these sensors are receivers. The second grid consists of 9 sensors, laid out 3×3 beginning at $(x, y) = (17480, 17480)$ m, with three receivers within a row 18520 m apart horizontally and three rows 18520 m apart vertically. The four sensors at the corners of this grid are co-located source/receiver units, and the remaining five sensors are receivers. Figures 6e and 6f contain the results obtained by applying the proposed algorithm to the first MSTWG Metron data set described above.

6. Conclusions and hints for future works

This work has addressed new trends in the field of multistatic sonar systems. Specifically, the focus is on the design and analysis of tracking algorithms capable of operating in highly noisy environments. The TBD approach is investigated and it is shown that TBD (or TBD-based) algorithms can overcome the limitations exhibited by the conventional trackers in case of low SNR targets or low-quality sensors. In fact, the class of decision schemes described in Subsection 3.1 guarantees good detection performance of weak moving targets and, as a byproduct, provides a rough estimate of the target locations, while the batch algorithm introduced in Subsection 3.2 ensures acceptable performance also when the probability of detection per sensor is low.
Several important issues would deserve further attention. First, observe that since the spectral properties of the noise may change with the distance from the sensor, the homogeneity assumption does not generally hold. In such a case, it would be important to assess the performance of the TBD algorithm proposed in Subsection 3.1 coupled with other possible estimates of the noise covariance matrix, like the so-called normalized sample covariance matrix, introduced in (Conte et al., EUSIPCO 1994), or the one introduced in (Conte et al., IEEE-TSP 2002). In addition, the Gaussian assumption is not always met in realistic scenarios and, hence, it would also be of interest a performance analysis in non-Gaussian disturbance.
Another key point that has not been sufficiently investigated is the design and the analysis of TBD (or TBD-based) algorithms for extended and/or multiple targets; a first work on the design of TBD algorithms for multiple targets has been presented in (S. Buzzi et al., IEEE-TAES 2008).

6.0.3 Acknowledgment
This work was made possible through collaboration between NURC, a NATO Research Centre, and Prof. Giuseppe Ricci, Dipartimento di Ingegneria dell'Innovazione, Università del Salento, Italy.

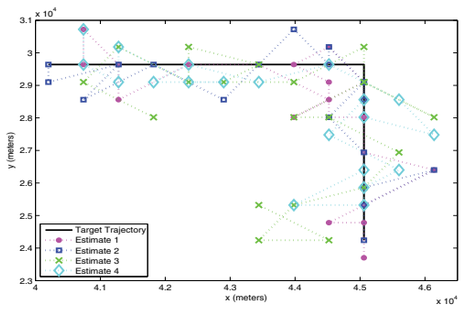

(a) Estimated tracks assuming $P_d = 0.3$.

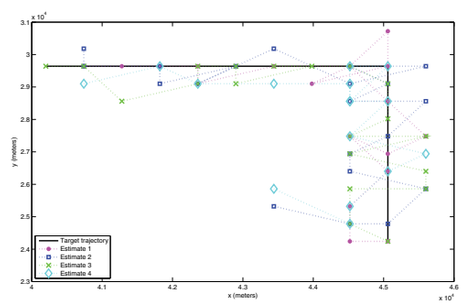

(b) Estimated tracks assuming $P_d = 0.5$.

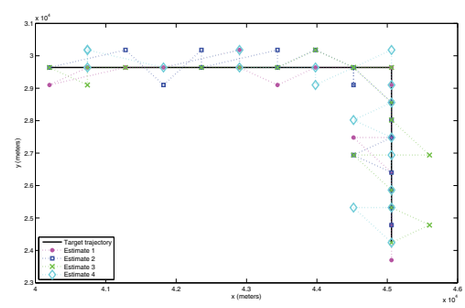

(c) Estimated tracks assuming $P_d = 0.8$.

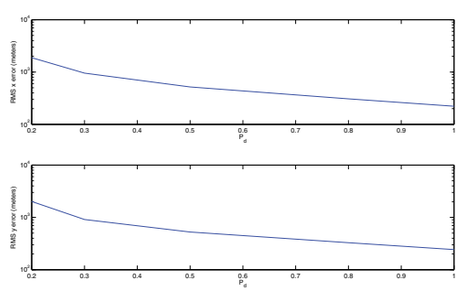

(d) RMS errors versus P_d.

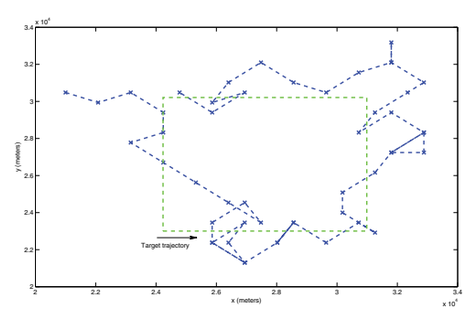

(e) Third target.

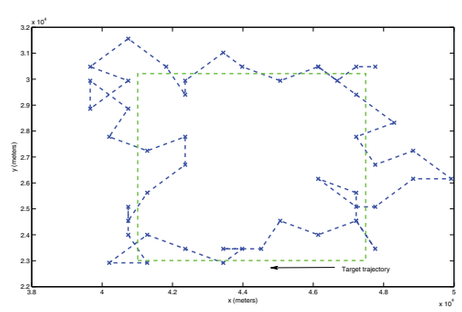

(f) Fourth target.

Fig. 6. Estimated tracks from 4 independent Monte Carlo trials, RMS errors, and estimated tracks from the first MSTWG Metron data set.

7. References

Daun, M. & Ehlers, F. (2010). Tracking Algorithms for Multistatic Sonar Systems. *EURASIP Journal on Advances in Signal Processing*, Vol. 2010, 2010.

Orlando, D.; Venturino, L.; Lops, M. & Ricci, G. (2010). Track-Before-Detect Strategies for STAP Radars. *IEEE Transactions on Signal Processing*, Vol. 58, No. 2, pp. 933-938, February 2010.

Orlando, D.; Ehlers, F. & Ricci, G. (2010). Track-before-detect Algorithms for Bistatic Sonars, *Proceedings of the 2nd International Workshop on Cognitive Information Processing*, Elba Island (Italy), June 2010.

Orlando, D.; Ehlers, F. & Ricci, G. (2010). A Maximum Likelihood Tracker for Multistatic Sonars, *Proceedings of the 13th International Conference on Information Fusion*, Edinburgh (UK), July 2010.

Orlov, K. (2009) *Description of the "MetronSimulation" data set for MSTWG*, Metron, Inc. Reston, Virginia, United States of America.

Willis, N. J. (2005) *Bistatic Radar*, Scitech Publishing Inc., 2005.

Bandiera, F; Orlando, D. & Ricci, G. (2009) *Advanced radar detection schemes under mismatched signal models*, Synthesis Lectures on Signal Processing No. 8, Morgan & Claypool Publishers, March 2009.

Varshney, P. R. (2005) *Distributed Detection and Data Fusion*, Springer-Verlag, New York, 1997.

Bar-Shalom, Y. & Fortmann, T. E. *Tracking and Data Association*, Academic Press, 1988.

Buzzi, S.; Lops, M. & Venturino, L. (2005). Track-before-detect procedures for early detection of moving target from airborne radars, *IEEE Transactions on Aerospace and Electronic Systems*, Vol. 41, No. 3, pp. 937-954, July 2005.

Buzzi, S.; Lops, M.; Venturino, L. & Ferri, M. (2008). Track-before-detect procedures in multi-targets environments, *IEEE Transactions on Aerospace and Electronic Systems*, Vol. 44, No. 3, pp. 1135-1150, July 2008.

Kramer, J. D. R. & Reid, J. W. S. (1990). Track-before-detect processing for an airborne type radar, *Proceedings of IEEE 1990 International Radar Conference*, Arlington, VA, USA, pp. 422-427, May 1990.

Wallace, W. R. (2002). The use of track-before-detect in pulse-doppler radar, *Proceedings of IEEE 2002 International Radar Conference*, Edinburgh, UK, pp. 315-319, October 2002.

Robey, F. C.; Fuhrman, D. L.; Kelly, E. J. & Nitzberg, R. (1992). A CFAR Adaptive Matched Filter Detector, *IEEE Transactions on Aerospace and Electronic Systems*, Vol. 29, No. 1, pp. 208-216, January 1992.

Forney, G. D. J. (1973). The Viterbi algorithm, *Proceedings of IEEE*, Vol. 29, No. 3, pp. 268-277, March 1973.

Bandiera, F.; Orlando, D. & Ricci, G. (2006). CFAR Detection of Extended and Multiple Point-like Targets without Assignment of Secondary Data, *IEEE Signal Processing Letters*, Vol. 13, No. 4, pp. 240-243, April 2006.

Urick, R. J. (1983) *Principles of underwater sound / 3d edition*, McGraw-Hill Inc., 1983.

Conte, E.; Lops, M. & Ricci, G. (2002). Adaptive Radar Detection in Compound-Gaussian Clutter. *Proceedings of Eusipco-94*, Edinburgh, UK, September 1994.

Conte, E.; De Maio, A. & Ricci, G. (2002). Recursive Estimation of the Covariance Matrix of a Compound-Gaussian Process and Its Application to Adaptive CFAR Detection, *IEEE Transactions on Signal Processing*, Vol. 50, No. 8, pp. 1908-1915, August 2002.

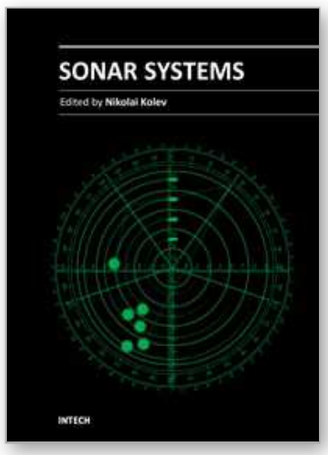

Sonar Systems

Edited by Prof. Nikolai Kolev

ISBN 978-953-307-345-3
Hard cover, 322 pages
Publisher InTech
Published online 12, September, 2011
Published in print edition September, 2011

The book is an edited collection of research articles covering the current state of sonar systems, the signal processing methods and their applications prepared by experts in the field. The first section is dedicated to the theory and applications of innovative synthetic aperture, interferometric, multistatic sonars and modeling and simulation. Special section in the book is dedicated to sonar signal processing methods covering: passive sonar array beamforming, direction of arrival estimation, signal detection and classification using DEMON and LOFAR principles, adaptive matched field signal processing. The image processing techniques include: image denoising, detection and classification of artificial mine like objects and application of hidden Markov model and artificial neural networks for signal classification. The biology applications include the analysis of biosonar capabilities and underwater sound influence on human hearing. The marine science applications include fish species target strength modeling, identification and discrimination from bottom scattering and pelagic biomass neural network estimation methods. Marine geology has place in the book with geomorphological parameters estimation from side scan sonar images. The book will be interesting not only for specialists in the area but also for readers as a guide in sonar systems principles of operation, signal processing methods and marine applications.

INTECH
open science | open minds

InTech Europe
University Campus STeP Ri
Slavka Krautzeka 83/A
51000 Rijeka, Croatia
Phone: +385 (51) 770 447
Fax: +385 (51) 686 166
www.intechopen.com

InTech China
Unit 405, Office Block, Hotel Equatorial Shanghai
No.65, Yan An Road (West), Shanghai, 200040, China
中国上海市延安西路65号上海国际贵都大饭店办公楼405单元
Phone: +86-21-62489820
Fax: +86-21-62489821

IntechOpen